Comparative analysis of nonperturbative effects in $B \to X_u l \bar{\nu}_l$ decays

Bernd A. Kniehl* and Gustav Kramer†

II. Institut für Theoretische Physik, Universität Hamburg, Luruper Chaussee 149, 22761 Hamburg, Germany

Ji-Feng Yang‡

Department of Physics, East China Normal University, 3663th Zhong Shan Bei Road, Shanghai 200062, China

(Received 22 March 2007; published 20 April 2007)

In order to extract the Cabibbo-Kobayashi-Maskawa matrix element $|V_{ub}|$ from $B \to X_u l \bar{\nu}_l$ decays, the overwhelming background from $B \to X_c l \bar{\nu}_l$ decays must be reduced by appropriate acceptance cuts. We study the nonperturbative effects due to the motion of the b quark inside the B meson on the phenomenologically relevant decay distributions of $B \to X_u l \bar{\nu}_l$ in the presence of such cuts in a comparative analysis based on shape functions and the parton model in the light cone limit. Comparisons with recent data from the CLEO, *BABAR*, and BELLE collaborations favor the shape-function approach.

DOI: 10.1103/PhysRevD.75.074023 PACS numbers: 12.39.Hg, 13.20.He, 14.40.Nd, 14.65.Fy

I. INTRODUCTION

To test the predictions of the standard model for the simultaneous violation of the charge conjugation and parity (CP) symmetries in B-meson decays, it is very important to know the matrix element $|V_{ub}|$ of the Cabibbo-Kobayashi-Maskawa quark-mixing matrix [1] very accurately. The uncertainties in existing measurements, by the CLEO [2], *BABAR* [3–6], and BELLE [7–9] collaborations, are dominantly due to uncertainties in the theoretical calculation of partial decay rates to be compared with the experimental measurements. Experimentally, the inclusive rate $\Delta\Gamma_{ul\nu}(\Delta\Phi)$ of $B \to X_u l \bar{\nu}_l$ decays in a restricted region $\Delta\Phi$ of phase space is measured, where the dominant charm background is suppressed and theoretical uncertainties are reduced. The theoretical factor $R(\Delta\Phi)$ directly relates the inclusive rate to $|V_{ub}|$ without extrapolation to the full phase space, as

$$|V_{ub}|^2 = \frac{\Delta\Gamma_{ul\nu}(\Delta\Phi)}{R(\Delta\Phi)}. \tag{1}$$

The uncertainties in the calculation of $R(\Delta\Phi)$ dominantly originate from the modeling of the Fermi motion of the b quark inside the B meson. Most of the recent analyses towards the determination of $|V_{ub}|$ from measurements of $\Delta\Gamma_{ul\nu}(\Delta\Phi)$ [4,5,8,9] rely on the calculation of $R(\Delta\Phi)$ by Lange *et al.* [10]. They use the so-called shape-function (SF) scheme, which is an extended version of the original SF approach [11,12] with many effects due to renormalization-group-improved perturbation theory, higher-order power corrections from subleading SF terms, etc. But there are many more approaches known for describing the nonperturbative $B \to b$ transition. We mention the Altarelli-Cabibbo-Corbo-Maiani-Martinelli (ACCMM) model [13], one of the oldest models to describe the motion of the b quark inside the B meson. In this model, it is assumed that the B meson consists of the b quark and a spectator quark, with definite mass $m_{\rm spec}$ and momentum $p_{\rm spec}$, which is considered quasifree. The b quark is treated as a virtual particle with a mass depending on $p_{\rm spec}$. Another popular model for describing the nonperturbative $B \to b$ transition is the model of Bareiss, Jin, Palmer, and Paschos based on the parton model approach in the light cone (LC) limit [14,15]. All these models, including the SF models, contain phenomenological functions of the respective variables describing the motion of the b quark inside the B meson with parameters fitted to the b-quark mass and one or two characteristic moments of these functions. Another approach tries to avoid these nonperturbative functions by assuming that the fragmentation of the B meson into the b quark and the spectator quark can be described as a radiation process off the b quark with a proper coupling inserted in the standard soft-gluon resummation formula [16]. An alternative approach, referred to as dressed-gluon exponentiation (DGE) in the literature [17], aims at combining a resummation of the perturbative expansion with a renormalon-based parametrization of power corrections in moment space.

Given the variety of approaches for treating the nonperturbative transition, it is desirable to make an attempt to compare these approaches with respect to their predictions for $R(\Delta\Phi)$ and other physical observables. In this work, we shall make such a comparison between the simple SF approach and the parton model approach in the LC limit, which we shall refer to as the LC approach in the following. Such a comparison of the parton model and the ACCMM model has already been done some time ago in Ref. [18].

The outline of this work is as follows. In Sec. II, we give a short introduction to the SF and LC approaches. Section III contains the results for $R(\Delta\Phi)$ for three choices of $\Delta\Phi$ underlying recent experimental measurements by *BABAR* and BELLE. In addition to $R(\Delta\Phi)$, we also present

*Electronic address: bernd.kniehl@desy.de
†Electronic address: gustav.kramer@desy.de
‡Electronic address: jfyang@phy.ecnu.edu.cn

in Sec. III distributions in several kinematical variables and compare them with measured differential decay distributions. Section IV contains a summary and the conclusions.

II. THEORETICAL INGREDIENTS

A. Perturbative differential decay rate

The differential decay width of $B \to X_u l \bar{\nu}_l$ has been calculated up to first order in the strong-coupling constant α_s by De Fazio and Neubert [19] using a fictitious gluon mass to regulate soft and collinear gluon contributions. This result has been confirmed using dimensional regularization for the soft and collinear singularities in Ref. [20] and by us. The quantity of interest is the triple differential decay rate $d^3\Gamma/(dx dz d\hat{p}^2)$ of

$$b(p_b) \to X_u(p) + l(p_l) + \bar{\nu}_l(p_\nu), \tag{2}$$

where $X_u = u$ or $X_u = u + g$ in the case of single-gluon emission and the assigned four-momenta are displayed in parentheses. Introducing $p = p_u + p_g$ and $q = p_l + p_\nu$, we have $p_b = p + q$. The variables x, z, and $\hat{p}^2$ are defined as

$$x = \frac{2p_b \cdot p_l}{m_b^2}, \qquad z = \frac{2p_b \cdot p}{m_b^2}, \qquad \hat{p}^2 = \frac{p^2}{m_b^2}, \tag{3}$$

and take the values

$$\begin{aligned} &0 \le x \le 1, \qquad \bar{x} \le z \le 1 + \bar{x}, \\ &\max(0, z-1) \le \hat{p}^2 \le \bar{x}(z - \bar{x}), \end{aligned} \tag{4}$$

where $\bar{x} = 1 - x$. The variable $\hat{p}^2$ measures the invariant mass square of the hadronic system X_u in units of m_b^2, while, in the b-quark rest frame, x and z correspond to the energies of l and X_u in units of $m_b/2$, respectively. For fixed values of z and $\hat{p}^2$, $\bar{x}$ varies in the range

$$\frac{z - \sqrt{z^2 - 4\hat{p}^2}}{2} \le \bar{x} \le \frac{z + \sqrt{z^2 - 4\hat{p}^2}}{2}. \tag{5}$$

Doubly and singly differential decay distributions are obtained by appropriately integrating over $d^3\Gamma/(dx dz d\hat{p}^2)$. The simplest distribution is the spectrum in x, which reads [19,21]:

$$\frac{1}{\Gamma_0}\frac{d\Gamma}{dx} = 2x^2(3-2x)\left[1 - \frac{C_F\alpha_s}{2\pi}G(x)\right], \tag{6}$$

where $C_F = 4/3$,

$$\Gamma_0 = \frac{G_F^2 |V_{ub}|^2 m_b^5}{192\pi^3}, \tag{7}$$

with G_F being Fermi's constant, is the total decay rate at leading order (LO) and

$$G(x) = \ln^2(1-x) + 2\mathrm{Li}_2(x) + \frac{2}{3}\pi^2 + \frac{82 - 153x + 86x^2}{12x(3-2x)} + \frac{41 - 36x + 42x^2 - 16x^3}{6x^2(3-2x)}\ln(1-x), \tag{8}$$

with Li_2 being the Spence function. By integrating over x, one obtains the well-known $\mathcal{O}(\alpha_s)$ formula for the total decay rate of $b \to X_u l \bar{\nu}_l$:

$$\Gamma = \Gamma_0\left[1 - \frac{C_F\alpha_s}{2\pi}\left(\pi^2 - \frac{25}{4}\right)\right]. \tag{9}$$

Formulas for other doubly differential distributions like $d^2\Gamma/(dz d\hat{p}^2)$ and $d^2\Gamma/(dx dz)$ or singly differential distributions like $d\Gamma/dz$ and $d\Gamma/d\hat{p}^2$ may be found in Ref. [19]. From $d^2\Gamma/(dz d\hat{p}^2)$, also the distribution in the hadronic invariant mass M_X can be calculated. In the heavy-quark limit, where $p_B = (M_B/m_b)p_b$, one has

$$M_X^2 = \hat{p}^2 m_b^2 + z m_b \bar{\Lambda} + \bar{\Lambda}^2, \tag{10}$$

where $\bar{\Lambda} = M_B - m_b$.

B. SF approach

In kinematic regions close to the phase space boundaries, the perturbative spectra are infrared sensitive and expected to receive large nonperturbative corrections. Such corrections are due to the motion of the b quark inside the B meson and are usually referred to as Fermi-motion corrections [13]. In the singly differential spectra, such regions are $1 - x = \mathcal{O}(\Lambda_{\mathrm{QCD}}/m_b)$ for the charged-lepton energy spectrum, $1 - z = \mathcal{O}(\Lambda_{\mathrm{QCD}}/m_b)$ for the hadronic energy spectrum, and the low-hadronic-mass region $M_X^2 = \mathcal{O}(\Lambda_{\mathrm{QCD}} m_b)$, where $\Lambda_{\mathrm{QCD}} \approx 0.5$ GeV is the asymptotic scale parameter of QCD.

One popular method to incorporate Fermi-motion effects is the introduction of a SF $F(k_+)$, which is supposed to describe light cone momentum distribution of the b quark inside the B meson [11,12]. The component k_+ of the b-quark light cone momentum varies between $-m_b$ and $\bar{\Lambda}$ with a distribution centered around $k_+ = 0$ and having a characteristic width of $\mathcal{O}(\bar{\Lambda})$. The physical B-meson decay distributions are calculated from a convolution of the perturbative b-quark decay spectra with $F(k_+)$. This is done by replacing the b-quark mass by the momentum-dependent mass $m_b + k_+$. Similarly, the parameter $\bar{\Lambda}$ is replaced by $\bar{\Lambda} - k_+$ [11]. Introducing $q_+ = \bar{\Lambda} - k_+$, the charged-lepton energy distribution, for example, is modified to become [19]

$$\frac{d\Gamma}{dE_l}(B \to X_u l \bar{\nu}_l) = 2\int_0^{M_B - 2E_l} dq_+ \frac{F(\bar{\Lambda} - q_+)}{M_B - q_+}\frac{d\Gamma(x_q)}{dx}, \tag{11}$$

where $d\Gamma/dx$ is the perturbative spectrum given in Eq. (6), $x_q = 2E_l/(M_B - q_+)$, and the charged-lepton energy E_l

varies in the range $0 \le E_l \le M_B/2$. The analogous formulas for the distributions in the total hadronic energy and the hadronic mass may be found in Ref. [19] and will not be repeated here. Since we wish to calculate the fractional decay rate with cuts on E_l and M_X, we need the doubly differential distribution $d^2\Gamma/(dE_l dM_X)$. This and the triply differential distribution $d^2\Gamma/(dE_l dM_X dq^2)$ are derived analogously to Eq. (11). After the implementation of the SF, the kinematic variables take values in the entire phase space determined by hadron kinematics. For example, the maximum lepton energy is $E_l^{\max} = M_B/2$, whereas it is equal to $m_b/2$ for the phase space of the perturbative decay rate.

Several functional forms of $F(k_+)$ are available in the literature. They are constrained through moments $A_n = \langle k_+^n \rangle$ of $F(k_+)$, which are related to the forward matrix elements of local operators on the light cone [10]. The first three moments are

$$A_0 = 1, \qquad A_1 = 0, \qquad A_2 = \frac{\mu_\pi^2}{3}, \tag{12}$$

where μ_π^2 is the average momentum square of the b quark inside the B meson [22]. In our analysis, we adopt the exponential form [23]

$$F(k_+) = N\left(1 - \frac{k_+}{\bar{\Lambda}}\right)^c e^{(1+c)k_+/\bar{\Lambda}}, \tag{13}$$

which obeys $A_1 = 0$ if one neglects terms exponentially small in $m_b/\bar{\Lambda}$. The condition $A_0 = 1$ fixes the normalization factor N, and the parameter c is related to the second moment as

$$A_2 = \frac{\bar{\Lambda}^2}{1+c}. \tag{14}$$

So, the b-quark mass m_b (or $\bar{\Lambda}$) and the parameter c (or μ_π^2) are the two input parameters of $F(k_+)$. Our choice of $\bar{\Lambda}$ and μ_π^2 will be specified in Sec. III, when we present our results for the cut-dependent partial decay rates $R(\Delta\Phi)$.

C. LC approach

Since the B meson is heavy, the momentum transferred in the decay to the final state is, in most regions of phase space, much larger than the energy of hadronic binding, which is of $\mathcal{O}(\Lambda_{\rm QCD})$. This suggests that the semileptonic decay of the B meson can be treated in a way analogous to deep-inelastic scattering (DIS) in lepton-proton collisions. There, LC dynamics dominates DIS and leads to the well-known scaling of the DIS structure functions. This is implemented in the parton model, where in LO the structure functions are given by the parton distribution functions. These are functions of the scaling variable ξ, which relates the parton four-momentum $p_q = \xi p_p$ to the proton four-momentum p_p. In an analogous manner, the hadron decay process $B \to X_u l \bar{\nu}_l$ is modeled by convoluting the parton decay process $b \to X_u l \bar{\nu}_l$ with the distribution function $f(\xi)$ of the momentum $p_b = \xi p_B$ of the b quark inside the B meson according to

$$d\Gamma(B \to X_u l \bar{\nu}_l) = \int d\xi f(\xi) d\Gamma(b \to X_u l \bar{\nu}_l)|_{p_b = \xi p_B}. \tag{15}$$

This has the consequence that $m_b = \xi M_B$ is also smeared with the variable ξ. The distribution function $f(\xi)$ can be expressed in terms of the matrix element of the LC bilocal b-quark operator between B-meson states as [24]

$$f(\xi) = \frac{1}{4\pi M_B^2} \int d(y \cdot p_B) e^{i\xi y \cdot p_B} \langle B|\bar{b}(0)\gamma \cdot p_B(1-\gamma_5) \times U(0,y) b(y)|B\rangle|_{y^2=0}, \tag{16}$$

where $U(0, y)$ is a gauge link associated with the background gluon field that ensures the gauge invariance of $f(\xi)$. The distribution function $f(\xi)$ is positive and has nonzero values for $0 \le \xi \le 1$ only. It fulfills three sum rules [24]. One of them is due to b-quark number conservation and reads

$$\int_0^1 d\xi f(\xi) = 1. \tag{17}$$

Reducing the bilocal operator in Eq. (16) to a local one with the help of the operator product expansion [24] in heavy-quark effective theory (HQET), one obtains two more sum rules. They determine, up to $\mathcal{O}(\Lambda_{\rm QCD}^2/m_b^2)$, the mean value μ and the variance σ^2 of $f(\xi)$, which characterize the position of the maximum and the width of the distribution [24]:

$$\mu = \int_0^1 d\xi \xi f(\xi) = \frac{m_b}{M_B}\left(1 + \frac{5}{3}E_b\right), \qquad \sigma^2 = \int_0^1 d\xi (\xi - \mu)^2 f(\xi) = \frac{m_b^2}{M_B^2}\left[\frac{2}{3}K_b - \left(\frac{5}{3}E_b\right)^2\right], \tag{18}$$

where

$$G_b = -\frac{1}{2M_B}\left\langle B \left| \bar{h}\frac{g_s G_{\alpha\beta}\sigma^{\alpha\beta}}{4m_b^2} h \right| B \right\rangle, \qquad K_b = -\frac{1}{2M_B}\left\langle B \left| \bar{h}\frac{(iD)^2}{2m_b^2} h \right| B \right\rangle, \qquad E_b = G_b + K_b. \tag{19}$$

Here, $g_s = \sqrt{4\pi\alpha_s}$, h is the b-quark field, $G_{\alpha\beta}$ is the field strength tensor of the strong force, and D is the covariant derivative involving the gluon field. The matrix elements G_b and K_b measure the chromomagnetic energy due to the b-quark spin and the kinetic energy of the b quark inside the B meson, respectively. Both are dimensionless HQET parameters of $\mathcal{O}(\Lambda_{\rm QCD}^2/m_b^2)$ and are often related to the alternative parameters

$$\lambda_1 = -2m_b^2 K_b, \qquad \lambda_2 = -\tfrac{2}{3}m_b^2 G_b. \tag{20}$$

The parameter λ_2 can be extracted from the B^*-B mass splitting yielding $\lambda_2 = (M_{B^*}^2 - M_B^2)/4 \approx 0.12\ \mathrm{GeV}^2$. Values for $\lambda_1 = -\mu_\pi^2$, introduced earlier, will be specified in Sec. III, when we present our results. If we introduce these two parameters in Eq. (18), we have

$$\mu = \frac{m_b}{M_B}\left(1 - \frac{5(\lambda_1 + 3\lambda_2)}{6m_b^2}\right),$$
$$\sigma^2 = \frac{m_b^2}{M_B^2}\left[-\frac{\lambda_1}{3m_b^2} - \left(\frac{5(\lambda_1 + 3\lambda_2)}{6m_b^2}\right)^2\right]. \tag{21}$$

Of course, the three parameters m_b, λ_1, and λ_2 only constrain the position of the maximum and the width of the distribution. For numerical evaluations, one needs the whole function $f(\xi)$, for which we adopt the ansatz [15,25]

$$f(\xi) = N\frac{\xi(1-\xi)}{a^2 + (\xi - b)^2}\theta(\xi)\theta(1-\xi). \tag{22}$$

The parameters a and b are determined from the values of μ and σ^2. The normalization factor N is fixed by Eq. (17). For $b = m_b/M_B$ and $a \to 0$, Eq. (22) becomes a delta function, namely $f(\xi) = \delta(\xi - m_b/M_B)$. In the following, we shall always use λ_1 and λ_2 as inputs to determine a and b via Eq. (21).

III. NUMERICAL RESULTS

The large background from $B \to X_c l\bar{\nu}_l$ is the main limitation for measuring $|V_{ub}|$. To reject this background, kinematic cuts have to be applied. Depending on these cuts, the acceptance for $B \to X_u l\bar{\nu}_l$ decays is reduced. With such acceptance cuts applied, the calculation of the $B \to X_u l\bar{\nu}_l$ decay rate is more complicated and, in particular, influenced much more strongly by the modeling of the nonperturbative $B \to b$ transition than without cuts.

In recent experimental analyses, four types of cuts have been introduced to separate $B \to X_u l\bar{\nu}_l$ decays from the much more abundant $B \to X_c l\bar{\nu}_l$ decays. First, various cuts on the charged-lepton energy E_l (with or without an additional cut on the invariant mass M_X of the hadronic system) were used by the CLEO [2], *BABAR* [4,5], and BELLE [8] collaborations. The three other cut scenarios, which were adopted by *BABAR* [3] and BELLE [7,9] and which we shall consider here, combine cuts on E_l with cuts on M_X, the invariant mass square q^2 of the leptonic system [26], and the variable $P_+ = E_X - |\vec{p}_X|$ [27], where E_X and $\vec{p}_X$ are the energy and three-momentum of the hadronic system X_u, respectively. Specifically, they are defined as: (1) $E_l > 1$ GeV, $M_X < 1.7$ GeV, and $q^2 > 8\ \mathrm{GeV}^2$; (2) $E_l > 1$ GeV and $M_X < 1.7$ GeV; and (3) $E_l > 1$ GeV and $P_+ < 0.66$ GeV. The corresponding fractional decay rates will be denoted as r_1, r_2, and r_3, respectively. They all depend on the description of the nonperturbative $b \to B$ transition, for which we shall use the SF and LC approaches as discussed in the previous section.

Both the SF $F(k_+)$ and the distribution function $f(\xi)$ of the LC approach depend strongly on the b-quark mass and much less on the parameters λ_1 and λ_2, as we shall see below. For these parameters, we choose $m_b = (4.72 \pm 0.08)$ GeV, $\lambda_1 = (-0.25 \pm 0.10)\ \mathrm{GeV}^2$, and $\lambda_2 = 0.12\ \mathrm{GeV}^2$. Since the b quark cannot be observed due to confinement, the value of m_b can only be obtained indirectly from measurements other than that of $B \to X_u l\bar{\nu}_l$. The value of m_b depends on the scheme, in which it is defined. For simplicity, we take m_b to be the pole mass. The scale-invariant b-quark mass in the modified minimal-subtraction ($\overline{\mathrm{MS}}$) scheme currently quoted by the Particle Data Group [28] as $\bar{m}_b = \bar{m}_b(\bar{m}_b) = (4.20 \pm 0.07)$ GeV corresponds to $m_b = (4.78 \pm 0.08)$ GeV at the two-loop level. A determination of m_b and λ_1 by fitting $B \to X_s\gamma$ decay spectra may be found in Ref. [29], with the result that $m_b = (4.79^{+0.06}_{-0.10})$ GeV and $\lambda_1 = (-0.24^{+0.09}_{-0.18})\ \mathrm{GeV}^2$. In the analysis of their data [9], the BELLE Collaboration used the values $m_b = 4.60$ GeV and $\lambda_1 = -0.20\ \mathrm{GeV}^2$ within the SF scheme. All these values are consistent with our above choice for m_b and λ_1. With these parameters, we calculate the parameters $\bar{\Lambda}$ and c that fix the SF $F(k_+)$ in Eq. (13) as well as, via Eq. (21), the parameters a and b that fix the distribution function $f(\xi)$ of the LC approach in Eq. (22). In the latter case, we also need as input the parameter λ_2, which we fix as described above. The values of $\bar{\Lambda}$ and c in Eq. (13) and those of a and b in Eq. (22) are collected in Tables I and II, respectively, for

TABLE I. Values of $\bar{\Lambda}$ (in GeV) and $c = -3\bar{\Lambda}^2/\lambda_1 - 1$ appearing in Eq. (13) for various values of m_b (in GeV) and λ_1 (in GeV^2).

m_b	4.64	4.72	4.80
$\bar{\Lambda}$	0.6392	0.5592	0.4792
λ_1			
−0.35	2.5021	1.6803	0.9683
−0.25	3.9029	2.7525	1.7556
−0.15	7.1715	5.2541	3.5927

TABLE II. Values of a and b appearing in Eq. (22) for various values of m_b (in GeV) and λ_1 (in GeV^2).

m_b	4.64	4.72	4.80	
λ_1				
−0.35	0.007 950	0.006 940	0.005 895	a
	0.8941	0.9094	0.9245	b
−0.25	0.005 911	0.005 215	0.004 493	a
	0.8861	0.9014	0.9166	b
−0.15	0.003 604	0.003 212	0.002 804	a
	0.8780	0.8934	0.9087	b

$m_b = 4.64$, 4.72, and 4.80 GeV and for $\lambda_1 = -0.35$, -0.25, and -0.15 GeV^2.

Before we can present our results for r_1, r_2, and r_3, we need to know the change of the fully integrated decay rate of $B \to X_u l \bar{\nu}_l$ due to the Fermi motion of the b quark inside the B meson. Therefore, we write

$$\Gamma(B \to X_u l \bar{\nu}_l) = r_0 \Gamma(b \to X_u l \bar{\nu}_l), \tag{23}$$

where $\Gamma(b \to X_u l \bar{\nu}_l)$ is given by Eq. (9) and the deviation of r_0 from unity measures the influence of the Fermi motion. The results for r_0 evaluated in the SF and LC approaches with the fixed value $\alpha_s = 0.22$ are given in Tables III and IV, respectively, for the same values of m_b and λ_1 as in Tables I and II. We see that, in both approaches, r_0 is approximately equal to one. The variation with m_b is very small; r_0 mostly depends on λ_1. The deviation of r_0 from unity is because the factor m_b in Γ_0 [see Eq. (7)] is replaced by $\langle m_b + k_+ \rangle^5$ in the SF case and by $\langle \xi m_b \rangle^5$ in the LC case. It is instructive to approximate these expectation values by their lowest nonvanishing moments. In the SF case, we thus obtain for r_0:

$$r_0 \approx 1 + \frac{10 A_2}{m_b^2}, \tag{24}$$

where A_2 is given in Eq. (14). This yields $r_0 = 1.0374$ for $m_b = 4.72$ GeV, almost the same value as in Table III. The deviation comes from the higher moments, which must be even smaller. Of course, these results do not imply that the integrated decay rate is almost independent of m_b. On the contrary, it is proportional to m_b^5 and, therefore, changes with this factor. Only the influence of the Fermi motion on this decay rate is small and feebly depends on m_b, as one would expect. Independently varying m_b and λ_1, we have $r_0 = 1.0353^{+0.0153}_{-0.0145}$. Table IV exhibits a similar pattern for r_0 in the LC case. For our central choice of m_b and λ_1, it is almost one. It changes very little with m_b and more with λ_1. Over the whole range of m_b and λ_1, we have $r_0 = 1.0044^{+0.0297}_{-0.0309}$. Approximating r_0 by the first two nonvanishing moments, we obtain

$$r_0 \approx 1 + \frac{25}{3} E_b + \frac{20}{3} K_b = 1 - \frac{45 \lambda_1}{6 m_b^2} - \frac{25 \lambda_2}{2 m_b^2}, \tag{25}$$

which yields $r_0 \approx 1.0168$ for our default values of m_b, λ_1, and λ_2. Comparison with Table IV reveals that, in the LC case, the higher moments are more important than in the SF case. Since the error of r_0 is doubled as compared to the SF case, the error in the integrated decay rate is also larger. From Tables III and IV, we may also conclude that parton-hadron duality is realized to good approximation for the total decay rate, r_0 being close to unity.

Next we present our results for the fractional decay rates r_1, r_2, and r_3. For the SF approach, they are listed in Table V for the same choices of m_b and λ_1 as above. The central values are $r_1 = 0.362$, $r_2 = 0.676$, and $r_3 = 0.602$. The results for the LC approach are given in Table VI, the central values being $r_1 = 0.360$, $r_2 = 0.694$, and $r_3 = 0.667$. They are similar to the SF case, except for r_3, which

TABLE III. Values of r_0 appearing in Eq. (23) evaluated for various values of m_b (in GeV) and λ_1 (in GeV^2) in the SF approach.

m_b / λ_1	4.64	4.72	4.80
-0.35	1.0506	1.0484	1.0463
-0.25	1.0369	1.0353	1.0338
-0.15	1.0225	1.0217	1.0208

TABLE IV. Values of r_0 appearing in Eq. (23) evaluated for various values of m_b (in GeV) and λ_1 (in GeV^2) in the LC approach.

m_b / λ_1	4.64	4.72	4.80
-0.35	1.0350	1.0335	1.0319
-0.25	1.0049	1.0044	1.0041
-0.15	0.9747	0.9755	0.9759

TABLE V. Values of r_1, r_2, and r_3 evaluated for various values of m_b (in GeV) and λ_1 (in GeV^2) in the SF approach.

m_b / λ_1	4.64	4.72	4.80	
	0.3438	0.3659	0.3860	r_1
-0.35	0.6283	0.6888	0.7398	r_2
	0.5411	0.6223	0.6908	r_3
	0.3386	0.3617	0.3824	r_1
-0.25	0.6082	0.6763	0.7330	r_2
	0.5076	0.6016	0.6796	r_3
	0.3347	0.3586	0.3795	r_1
-0.15	0.5828	0.6633	0.7290	r_2
	0.4614	0.5779	0.6724	r_3

TABLE VI. Values of r_1, r_2, and r_3 evaluated for various values of m_b (in GeV) and λ_1 (in GeV^2) in the LC approach.

m_b / λ_1	4.64	4.72	4.80	
	0.3476	0.3674	0.3856	r_1
-0.35	0.6201	0.7305	0.7878	r_2
	0.5668	0.6997	0.7657	r_3
	0.3395	0.3601	0.3788	r_1
-0.25	0.5578	0.6942	0.7743	r_2
	0.4584	0.6674	0.7520	r_3
	0.3313	0.3527	0.3720	r_1
-0.15	0.4945	0.6300	0.7557	r_2
	0.1886	0.6192	0.7357	r_3

is larger in the LC case. The SF to LC ratios read 1.00, 0.97, and 0.90. Thus, the fractional decay rates are remarkably similar in the two approaches and differ only slightly from the results $r_1 = 0.34$, $r_2 = 0.66$, and $r_3 = 0.57$ obtained in Ref. [10], which were used in Ref. [30] to determine $|V_{ub}|$ through a global analysis of the available experimental data. As expected, the values of r_1, r_2, and r_3 depend much more strongly on m_b than on λ_1, both in the SF and LC approaches. The variations of r_i with these two parameters are larger in the LC approach than in the SF approach. If we express these variations as errors, we have $r_1 = 0.362^{+0.024}_{-0.027}$, $r_2 = 0.676^{+0.064}_{-0.094}$, and $r_3 = 0.602^{+0.089}_{-0.140}$ in the SF approach and $r_1 = 0.360^{+0.026}_{-0.029}$, $r_2 = 0.694^{+0.094}_{-0.200}$, and $r_3 = 0.667^{+0.098}_{-0.479}$ in the LC approach. We notice that, in the LC approach, r_3 becomes abnormally small for $m_b = 4.64$ GeV and $\lambda_1 = -0.15$ GeV^2.

The similarity of the fractional decay rates r_1, r_2, and r_3 in the two approaches considered here might be related to a fortunate choice of the cut parameters $E_l^{\min}$, $M_X^{\max}$, $(q^2)^{\min}$, and $P_+^{\max}$, whereas the distributions in M_X, q^2, and P_+ for a fixed value of $E_l^{\min} = 1$ GeV say, could differ significantly. To elucidate this point, we calculate the partial decay fractions r_1, r_2, and r_3 as functions of the cut parameters $M_X^{\max}$, $(q^2)^{\min}$, and $P_+^{\max}$ for the default values of the input parameters, $m_b = 4.72$ GeV ($\bar{\Lambda} = 0.5592$ GeV) and $\lambda_1 = -0.25$ GeV^2. For this purpose, we define

$$\tilde{r}_1((q^2)^{\max}) = \frac{1}{\Gamma}\int_0^{(q^2)^{\max}} dq^2 \frac{d\Gamma}{dq^2}\bigg|_{E_l>1\ \mathrm{GeV}, M_X<1.7\ \mathrm{GeV}}, \tag{26}$$

$$\tilde{r}_2(M_X^{\max}) = \frac{1}{\Gamma}\int_0^{M_X^{\max}} dM_X \frac{d\Gamma}{dM_X}\bigg|_{E_l>1\ \mathrm{GeV}}, \tag{27}$$

$$\tilde{r}_3(P_+^{\max}) = \frac{1}{\Gamma}\int_0^{P_+^{\max}} dP_+ \frac{d\Gamma}{dP_+}\bigg|_{E_l>1\ \mathrm{GeV}}, \tag{28}$$

which are related to r_1, r_2, and r_3 as

$$\begin{aligned} r_1 &= \tilde{r}_1(26\ \mathrm{GeV}^2) - \tilde{r}_1(8\ \mathrm{GeV}^2), \\ r_2 &= \tilde{r}_2(1.7\ \mathrm{GeV}), \\ r_3 &= \tilde{r}_3(0.66\ \mathrm{GeV}). \end{aligned} \tag{29}$$

In Fig. 1, $\tilde{r}_1$ is plotted as a function of $(q^2)^{\max}$ for the SF and LC approaches. We observe that the difference between the two approaches is rather small over the whole range of $(q^2)^{\max}$, way up to 25 GeV^2. Later, when we compare with experimental measurements, we shall see that the same holds true for the normalized distribution $(1/\Gamma)d\Gamma/dq^2$ with the above cuts on E_l and M_X. The situation is very similar for $\tilde{r}_2$, which is shown as a function of $M_X^{\max}$ in Fig. 2. Here, the difference between the two approaches is appreciable only for small values of $M_X^{\max}$, for $M_X^{\max} \lesssim 1.5$ GeV. The situation is very different for $\tilde{r}_3$, which is depicted as a function of $P_+^{\max}$ for the two approaches in

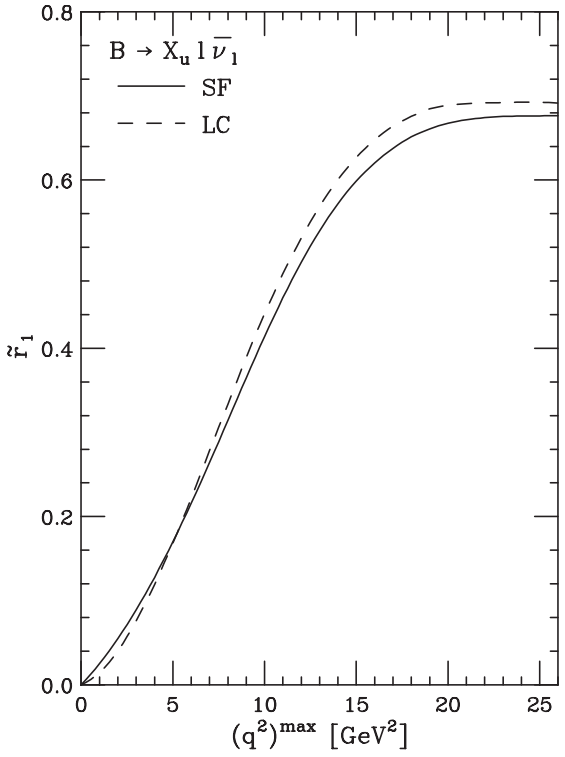

FIG. 1. Fractional decay rate $\tilde{r}_1$ defined in Eq. (26) evaluated as a function of $(q^2)^{\max}$ in the SF (solid line) and LC (dashed line) approaches.

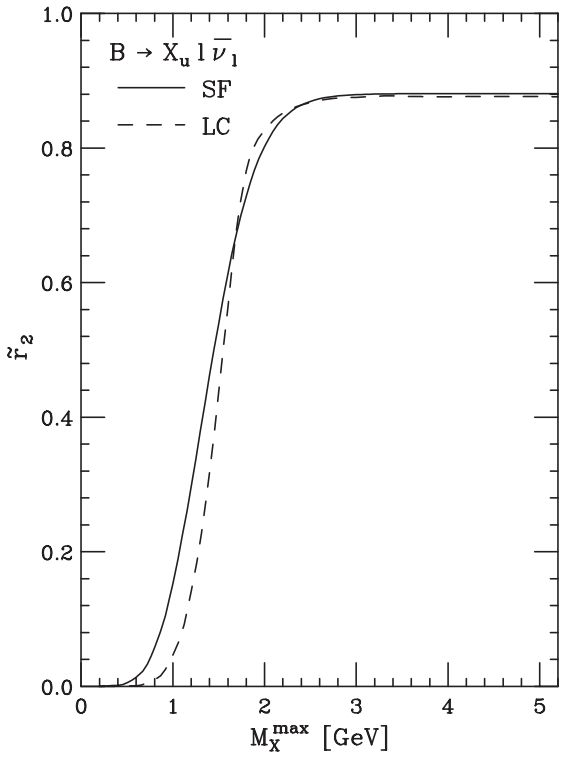

FIG. 2. Fractional decay rate $\tilde{r}_2$ defined in Eq. (27) evaluated as a function of $M_X^{\max}$ in the SF (solid line) and LC (dashed line) approaches.

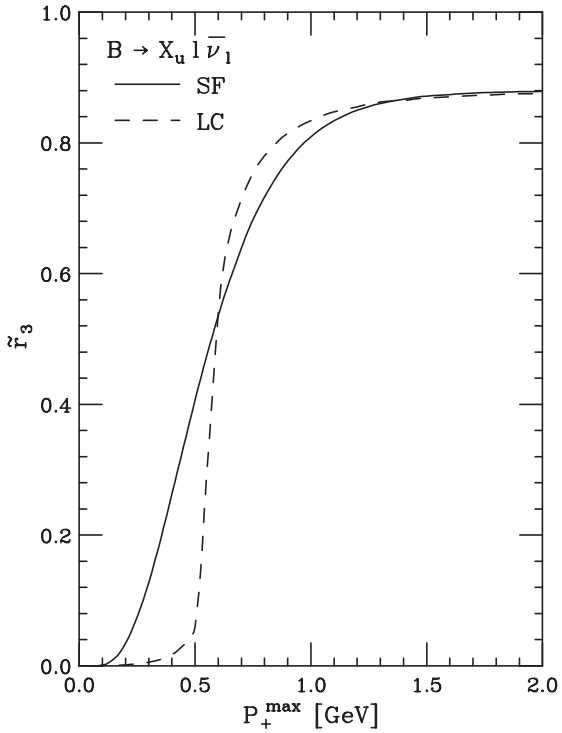

FIG. 3. Fractional decay rate $\tilde{r}_3$ defined in Eq. (28) evaluated as a function of $P_+^{\max}$ in the SF (solid line) and LC (dashed line) approaches.

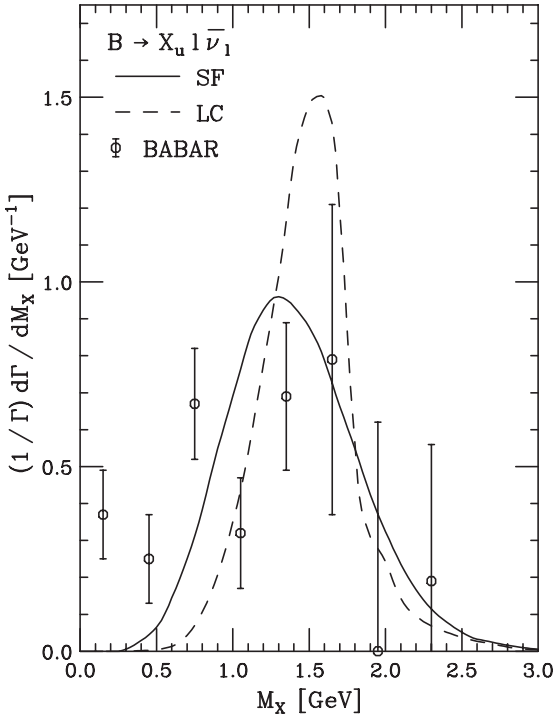

FIG. 4. The decay distribution $(1/\Gamma)d\Gamma/dM_X$ with $E_l > 1$ GeV normalized to unity in the signal region ($M_X < 2.5$ GeV) as predicted in the SF (solid line) and LC (dashed line) approaches is compared with *BABAR* data [6].

Fig. 3. We observe that the two distributions coincide at $P_+^{\max} \approx 0.6$ GeV, where their slopes are very different, however. The result of the LC approach is somewhat larger above this value of $P_+^{\max}$, way up to $P_+^{\max} \approx 1.2$ GeV, while it is significantly smaller below. As we shall illustrate below, this may be understood by considering the normalized P_+ distribution $(1/\Gamma)d\Gamma/dP_+$ with the cut $E_l > 1$ GeV, which is very different for the two approaches. It turns out that the choice of $E_l^{\min}$ is not responsible for this difference.

As for measurements of fractional decay rates $R(\Delta\Phi)$, experimental data for the normalized distributions $(1/\Gamma)d\Gamma/dM_X$ and $(1/\Gamma)d\Gamma/dP_+$ with cuts on E_l have been published and can be compared to the respective distributions evaluated in the SF and LC approaches (see Ref. [16] for a similar comparison). Specifically, $(1/\Gamma)d\Gamma/dM_X$ distributions with $E_l > 1$ GeV have been published by *BABAR* [3,6] and BELLE [9]. In Figs. 4 and 5, we compare these measured distributions to our predictions in the SF and LC approaches. Both the measured and predicted distributions are normalized to unity in the signal region, which is defined by $M_X < 2.5$ GeV for *BABAR* [6] and by $M_X < 1.7$ GeV for BELLE [9]. From Figs. 4 and 5, we see that the predictions in the SF approach are in reasonable agreement with both measurements, whereas the distributions of the LC approach are much too narrow and their peaks are much higher than in the measured distributions. A similar comparison is performed in

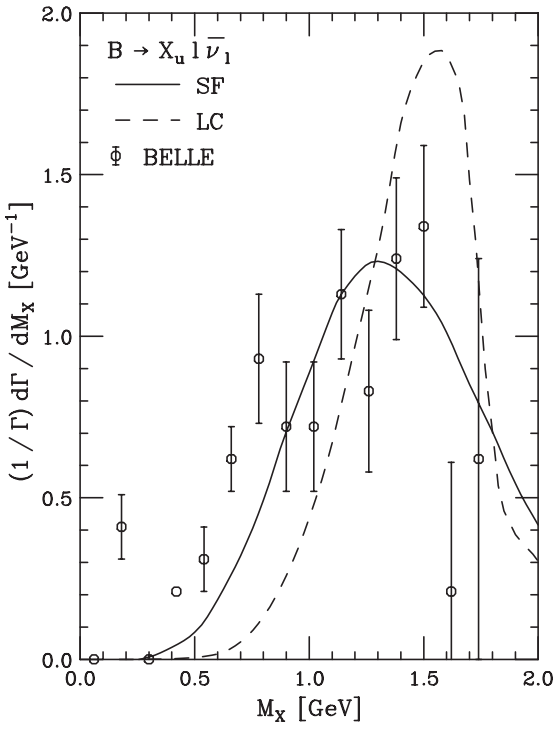

FIG. 5. The decay distribution $(1/\Gamma)d\Gamma/dM_X$ with $E_l > 1$ GeV normalized to unity in the signal region ($M_X < 1.7$ GeV) as predicted in the SF (solid line) and LC (dashed line) approaches is compared with BELLE data [9].

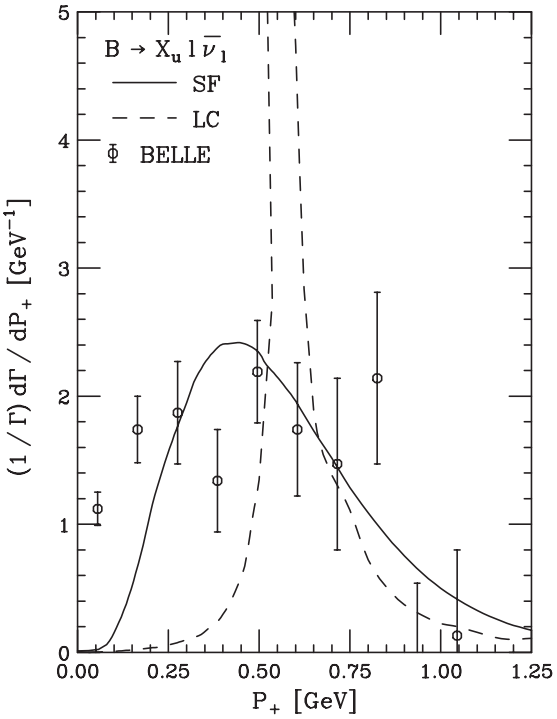

FIG. 6. The decay distribution $(1/\Gamma)d\Gamma/dP_+$ with $E_l > 1$ GeV normalized to unity in the signal region ($P_+ < 0.66$ GeV) as predicted in the SF (solid line) and LC (dashed line) approaches is compared with BELLE data [9].

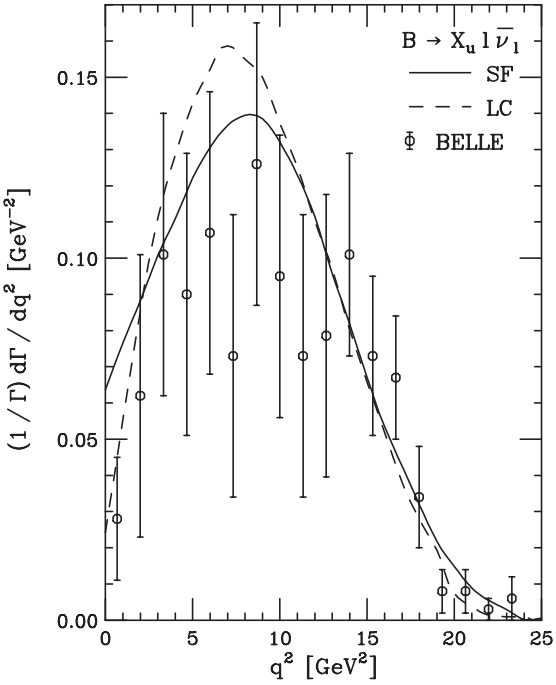

FIG. 7. The decay distribution $(1/\Gamma)d\Gamma/dq^2$ with $E_l > 1$ GeV normalized to unity in the signal region ($M_X < 1.7$ GeV and $q^2 > 8$ GeV^2) as predicted in the SF (solid line) and LC (dashed line) approaches is compared with BELLE data [9].

Fig. 6 for the normalized distribution $(1/\Gamma)d\Gamma/dP_+$ with $E_l > 1$ GeV measured by BELLE [9]. Both the measured and calculated distributions are normalized to unity in the signal region defined by $P_+ < 0.66$ GeV. Again, the distribution in the SF approach agrees more or less with the experimental data, whereas the one in the LC approach is much too narrow. BELLE [9] also presented experimental data on the normalized distribution $(1/\Gamma)d\Gamma/dq^2$ with $E_l > 1$ GeV normalized to unity in the signal region defined by $M_X < 1.7$ GeV and $q^2 > 8$ GeV^2. These are compared in Fig. 7 with the predictions based on the SF and LC approaches. Here, the two theoretical distributions are very similar and both agree with the measurement reasonably well.

Finally, we turn to the charged-lepton energy distribution $d\Gamma/dE_l$. In analogy to Eqs. (26)–(28), we define the fractional decay rate

$$\tilde{r}_4(E_l^{\max}) = \frac{1}{\Gamma}\int_0^{E_l^{\max}} dE_l \frac{d\Gamma}{dE_l}. \tag{30}$$

In Tables VII and VIII, we present the values of $\tilde{r}_4(2.3\ \text{GeV})$ evaluated for various values of m_b and λ_1 in the SF and LC approaches, respectively. We notice that, for given values of m_b and λ_1, the results in the two approaches differ appreciably. In particular, $\tilde{r}_4(2.3\ \text{GeV})$ depends much more strongly on m_b for fixed λ_1 and vice versa in the LC approach as compared to the SF approach.

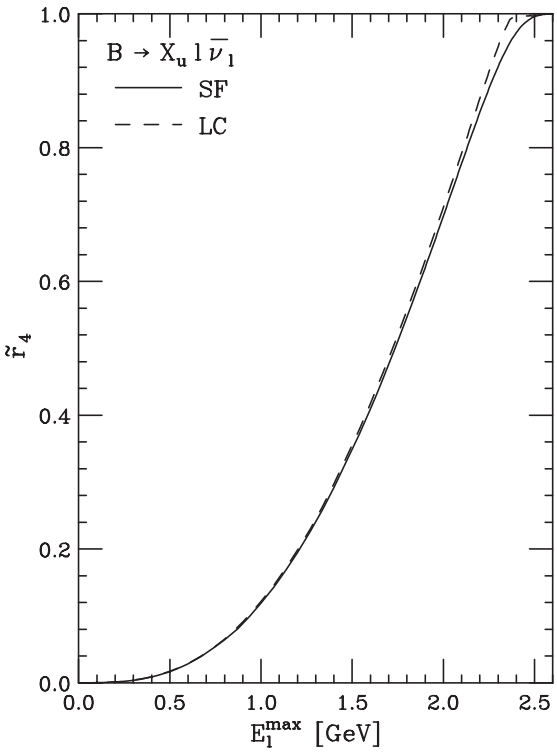

FIG. 8. Fractional decay rate $\tilde{r}_4$ defined in Eq. (30) evaluated as a function of $E_l^{\max}$ in the SF (solid line) and LC (dashed line) approaches.

TABLE VII. Values of $\tilde{r}_4(2.3\ \mathrm{GeV})$ defined in Eq. (30) evaluated for various values of m_b (in GeV) and λ_1 (in GeV^2) in the SF approach.

m_b / λ_1	4.64	4.72	4.80
−0.35	0.9307	0.9099	0.8874
−0.25	0.9419	0.9210	0.8978
−0.15	0.9558	0.9347	0.9107

TABLE VIII. Values of $\tilde{r}_4(2.3\ \mathrm{GeV})$ defined in Eq. (30) evaluated for various values of m_b (in GeV) and λ_1 (in GeV^2) in the LC approach.

m_b / λ_1	4.64	4.72	4.80
−0.35	0.9646	0.9385	0.9106
−0.25	0.9780	0.9524	0.9241
−0.15	0.9910	0.9669	0.9382

This is due to the fact that the E_l distribution falls off much more rapidly towards the threshold at $E_l^{\max} = M_B/2$ in the LC approach as compared to the SF approach (see Figs. 9–11). Of course, this effect diminishes if $E_l^{\max}$ is taken to be smaller than 2.3 GeV. In this case, also the sensitivity of $\tilde{r}_4(E_l^{\max})$ on m_b and λ_1 is reduced. The SF result for $\tilde{r}_4(2.3\ \mathrm{GeV})$ agrees quite well with the value used by CLEO [2] to determine $|V_{ub}|$ from the data points in the range $2.3\ \mathrm{GeV} < E_l < 2.6\ \mathrm{GeV}$.

In Fig. 8, $\tilde{r}_4$ is displayed as a function of $E_l^{\max}$ for the SF (solid line) and LC (dashed line) approaches. We observe that, as $E_l^{\max}$ approaches its kinematical upper limit, the LC result is saturated appreciably earlier than the SF one. This would lead to an according difference in the value of $|V_{ub}|$ extracted from the data if a large $E_l^{\max}$ cut were imposed. For $E_l^{\max} \lesssim 2$ GeV, the SF and LC results for $\tilde{r}_4$ are very similar.

In Figs. 9–11, we compare the normalized E_l distributions $(1/\Gamma)d\Gamma/dE_l$ predicted by the SF and LC approaches with measurements by CLEO [2], *BABAR* [5], and BELLE [8], respectively. Both the measured and calculated distributions are normalized to unity in the signal region, which is defined by $E_l > 2.30$ GeV for CLEO [2] and by $E_l > 2.25$ GeV for *BABAR* [5] and BELLE [8]. In the signal region, where the background from $b \to c$ transitions is expected to be minimal, the SF results agree with the CLEO, *BABAR*, and BELLE data quite satisfactorily, while the LC results are clearly disfavored. In fact, the E_l distributions of the LC approach drop off much too strongly towards the threshold at $E_l = M_B/2$ and deviate from the data throughout the signal region. This disagreement again points to the inadequacy of the LC approach to describe the nonperturbative effects in $B \to X_u l \bar{\nu}_l$ decays, which was already noticed for the M_X and P_+ distributions in Figs. 4–

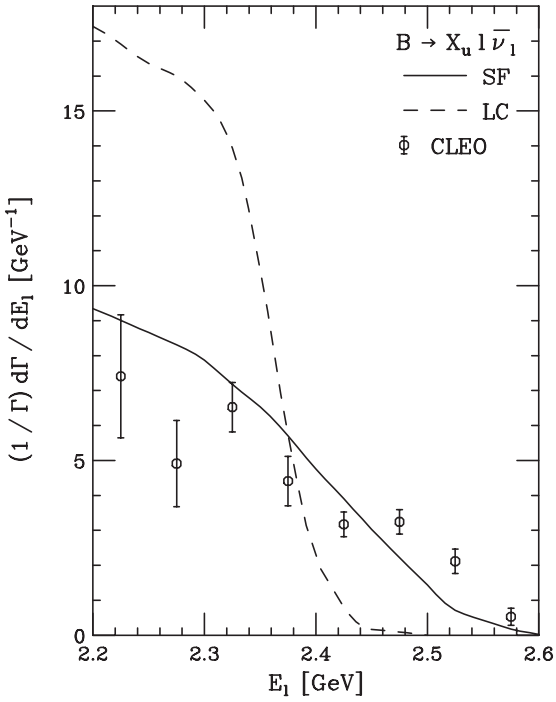

FIG. 9. The decay distribution $(1/\Gamma)d\Gamma/dE_l$ normalized to unity in the signal region ($2.30\ \mathrm{GeV} < E_l < 2.60\ \mathrm{GeV}$) as predicted in the SF (solid line) and LC (dashed line) approaches is compared with CLEO data [2].

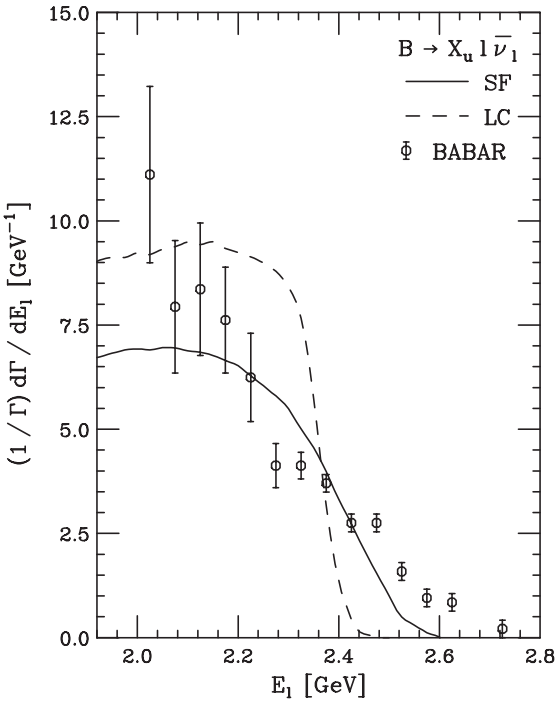

FIG. 10. The decay distribution $(1/\Gamma)d\Gamma/dE_l$ normalized to unity in the signal region ($2.25\ \mathrm{GeV} < E_l < 2.60\ \mathrm{GeV}$) as predicted in the SF (solid line) and LC (dashed line) approaches is compared with *BABAR* data [5].

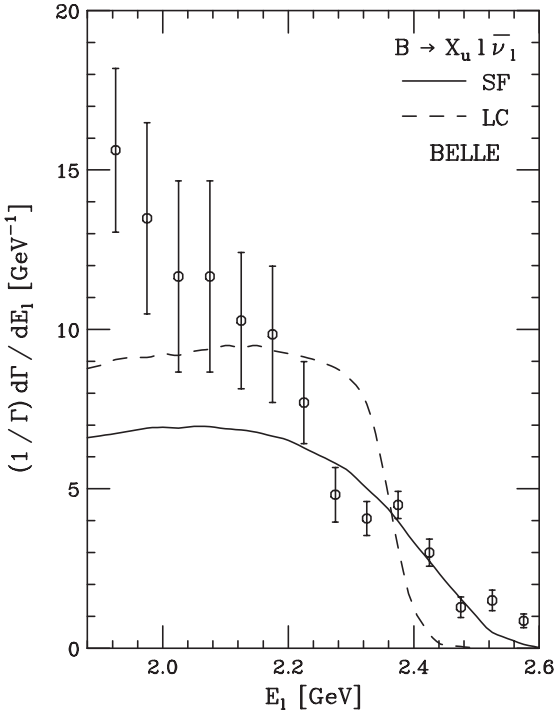

FIG. 11. The decay distribution $(1/\Gamma)d\Gamma/dE_l$ normalized to unity in the signal region (2.25 GeV $< E_l <$ 2.60 GeV) as predicted in the SF (solid line) and LC (dashed line) approaches is compared with BELLE data [8].

6. Finally, we should note that, in Figs. 9–11, the theoretical predictions refer to the rest frame of the B meson, while the experimental data refer to that of the $\Upsilon(4S)$ meson. However, since the motion of the B mesons in the $\Upsilon(4S)$ rest frame is nonrelativistic, this mismatch is rather insignificant in comparison with the experimental errors.

IV. CONCLUSIONS

We studied nonperturbative effects on $B \to X_u l\bar{\nu}_l$ decays due to the motion of the b quark inside the B meson adopting two approaches frequently discussed in the literature, namely, the shape-function formalism and the parton model in the light cone limit. While these effects are generally small for the total decay rate, they may become substantial once kinematic acceptance cuts are applied. In fact, such acceptance cuts are indispensable in practice in order to suppress the overwhelming background from $B \to X_c l\bar{\nu}_l$ decays. We considered three cut scenarios, involving the invariant mass M_X of the hadronic system X_u, the variable $P_+ = E_X - |\vec{p}_X|$ related to the energy E_X and the three-momentum $\vec{p}_X$ of X_u, the invariant mass square q^2 of the leptonic system, and the charged-lepton energy E_l, that were adopted in recent experimental analyses by the CLEO, *BABAR*, and BELLE collaborations. Comparisons with decay distributions in M_X, P_+, and E_l measured in these experiments disfavor the light cone approach.

ACKNOWLEDGMENTS

The work of B. A. K. and G. K. was supported in part by the German Federal Ministry of Education and Research (BMBF) through Grant No. 05 HT6GUA. The work of J.-F. Y. was supported in part by the National Natural Science Foundation of China through Grants No. 10205004 and No. 10475028.

[1] N. Cabibbo, Phys. Rev. Lett. **10**, 531 (1963); M. Kobayashi and T. Maskawa, Prog. Theor. Phys. **49**, 652 (1973).
[2] A. Bornheim *et al.* (CLEO Collaboration), Phys. Rev. Lett. **88**, 231803 (2002).
[3] B. Aubert *et al.* (*BABAR* Collaboration), Phys. Rev. Lett. **92**, 071802 (2004); Report No. BABAR-CONF-05/11, No. SLAC-PUB-11310 (hep-ex/0507017).
[4] B. Aubert *et al.* (*BABAR* Collaboration), Phys. Rev. Lett. **95**, 111801 (2005); **97**, 019903(E) (2006).
[5] B. Aubert *et al.* (*BABAR* Collaboration), Phys. Rev. D **73**, 012006 (2006).
[6] B. Aubert *et al.* (*BABAR* Collaboration), Phys. Rev. Lett. **96**, 221801 (2006).
[7] H. Kakuno *et al.* (BELLE Collaboration), Phys. Rev. Lett. **92**, 101801 (2004).
[8] A. Limosani *et al.* (BELLE Collaboration), Phys. Lett. B **621**, 28 (2005).
[9] I. Bizjak *et al.* (BELLE Collaboration), hep-ex/0505088; published without Fig. 3(b) in Phys. Rev. Lett. **95**, 241801 (2005).
[10] B. O. Lange, M. Neubert, and G. Paz, Phys. Rev. D **72**, 073006 (2005).
[11] M. Neubert, Phys. Rev. D **49**, 3392 (1994); **49**, 4623 (1994); T. Mannel and M. Neubert, *ibid.* **50**, 2037 (1994).
[12] I. I. Bigi, M. A. Shifman, N. G. Uraltsev, and A. I. Vainshtein, Int. J. Mod. Phys. A **9**, 2467 (1994); I. Bigi, M. Shifman, N. Uraltsev, and A. Vainshtein, Phys. Lett. B **328**, 431 (1994).
[13] G. Altarelli, N. Cabibbo, G. Corbo, L. Maiani, and G. Martinelli, Nucl. Phys. **B208**, 365 (1982).
[14] A. Bareiss and E. A. Paschos, Nucl. Phys. **B327**, 353 (1989); C. H. Jin, W. F. Palmer, and E. A. Paschos, Phys. Lett. B **329**, 364 (1994).
[15] C. Jin and E. A. Paschos, in *Proceedings of the International Symposium on Heavy Flavor and Electroweak Theory, Beijing, China, 1995*, edited by C.-H. Chang and C.-S. Huang (World Scientific, Singapore, 1996) p. 132.

[16] U. Aglietti, G. Ferrera, and G. Ricciardi, Nucl. Phys. **B768**, 85 (2007); and earlier papers by these authors cited therein.
[17] J. R. Andersen and E. Gardi, J. High Energy Phys. 01 (2006) 097; 01 (2007) 029.
[18] C. S. Kim, Y. G. Kim, and K. Y. Lee, Phys. Rev. D **57**, 4002 (1998).
[19] F. De Fazio and M. Neubert, J. High Energy Phys. 06 (1999) 017.
[20] H. Kim, Ph.D thesis, University of Hamburg [Report No. DESY-THESIS-2002-048 (unpublished)].
[21] M. Jezabek and J. H. Kühn, Nucl. Phys. **B320**, 20 (1989).
[22] A. F. Falk and M. Neubert, Phys. Rev. D **47**, 2965 (1993).
[23] A. L. Kagan and M. Neubert, Eur. Phys. J. C **7**, 5 (1999).
[24] C. Jin, Eur. Phys. J. C **11**, 335 (1999).
[25] C. Jin and E. A. Paschos, Eur. Phys. J. C **1**, 523 (1998).
[26] C. W. Bauer, Z. Ligeti, and M. E. Luke, Phys. Rev. D **64**, 113004 (2001).
[27] S. W. Bosch, B. O. Lange, M. Neubert, and G. Paz, Phys. Rev. Lett. **93**, 221801 (2004).
[28] W. M. Yao *et al.* (Particle Data Group), J. Phys. G **33**, 1 (2006).
[29] B. Aubert *et al.* (*BABAR* Collaboration), Phys. Rev. D **72**, 052004 (2005).
[30] E. Barberio *et al.* (Heavy Flavor Averaging Group (HFAG)), hep-ex/0603003.